ARTICLE IN PRESS

Available online at www.sciencedirect.com

ScienceDirect

Advances in Space Research xxx (xxxx) xxx

ADVANCES IN SPACE RESEARCH (a COSPAR publication)

www.elsevier.com/locate/asr

World grid of cosmic ray vertical cut-off rigidity for the last decade

M. Gerontidou [a,*], N. Katzourakis [a], H. Mavromichalaki [a], V. Yanke [b], E. Eroshenko [b]

[a] Nuclear and Particle Physics Department, Faculty of Physics, National and Kapodistrian, University of Athens, Athens, Greece
[b] Institute of Terrestrial Magnetism, Ionosphere and Radiowave Propagation of Russian Academy of Science, IZMIRAN, Moscow, Russia

Received 6 November 2020; received in revised form 4 January 2021; accepted 6 January 2021

Abstract

Cosmic ray cut-off rigidity tables and maps over the world concerning the epochs 2010, 2015 and the current one 2020 have been constructed. These maps display the effective cut-off rigidity in every five degrees in latitude and in longitude at the altitude of 20 km above the surface of the international reference ellipsoid. The values of the geomagnetic cut-off rigidity were calculated in every 5° in latitude and in every 15° in longitude applying the well-known method of particle trajectory calculations resulted from the theory of the particle motion in the Earth's magnetic field. The applied software employed the 12th Generation of the International Geomagnetic Reference Field (IGRF 12) and trajectories were calculated at 0.01 GV intervals in order to determine the vertical cut-off rigidity for each location. Beyond the use of the calculated cut-off rigidity values as a basic reference of charged particle access to different geographical locations during quiet and/or more intense geomagnetic periods, these results can be used for a long- term forecasting of the geomagnetic conditions variations.

Keywords: Cut-off rigidity; Cosmic ray; Geomagnetic rigidity cut-off

1. Introduction

The secular variation in the geomagnetic field and its effect on cosmic radiation measurements have been extensively studied in a previous work by Shea and Smart (1990). Modern requirements for an experiment in the field of solar-terrestrial physics need a thorough study of it. First of all, this is due to the fact that over a half-century observational period of cosmic rays (since the year 1957), the geomagnetic field was decreased by an average of 4% (Gvozdevsky et al., 2019). On the contrary, it is noted that at the same time the contribution of the high harmonics of the geomagnetic field over the period under consideration, was increased by 29%. In addition, magnetic anomalies have a general tendency to drift westward at approximately 0.15°/year (Zi-Gang and Xu,2001).

In order to evaluate the consequences of such a large restructuring of the magnetic field in terms of the magnetospheric effects of cosmic rays for practical purposes, such as the assessment of radiation exposure (Tezari et al., 2020), it is necessary:

(a) to obtain planetary distributions of the geomagnetic cut-off rigidity for a network of stations for the entire observational period;
(b) to evaluate the long-term changes in the geomagnetic cut-off of cosmic rays retrospectively and make a forecast for the near future;
(c) to estimate the expected secular variations of the neutron and muon components of cosmic rays due to geomagnetic variations.

It is well-known that the geomagnetic field (GMF) serves as a natural shield against primary cosmic rays. In this sense, the geomagnetic cut-off rigidities are considered

* Corresponding author.
E-mail address: mgeront@phys.uoa.gr (M. Gerontidou).

https://doi.org/10.1016/j.asr.2021.01.011
0273-1177/

as a quantitative measure of the shielding provided by the Earth's magnetic field. The cut-off rigidity Rc (θ, φ) at a selected location is defined as the lowest rigidity which a charged particle must possess in order to reach at this specific point on the Earth's surface from the direction specified by the zenith θ and azimuth φ angles of arrival at the top of the atmosphere (Shea et al., 1965). The determination of the geomagnetic cut-off rigidity is defined by trajectory calculations at discrete rigidity intervals, beginning at a value above the highest possible cut-off, and progress down in steps through a rigidity spectrum scan until the lowest possible allowed trajectory called the upper cut-off. Then the first discontinuity in the asymptotic direction, i.e., the first obtained forbidden trajectory is the start of the cosmic ray penumbra. The last allowed trajectory identifies the lower end of the cosmic ray penumbra, the lower cut-off. The effective cut-off rigidity, R_{eff}, is then a weighted average between the upper and the lower cut-off rigidities (Bütikofer, 2018).

Nevertheless, the cut-off rigidity at a specific point at the top of the atmosphere is featured by the minimum rigidity for which cosmic rays can arrive at that point fromthe zenith. This rigidity defined as the vertical cut-off rigidity and varies from zero at the geomagnetic poles to ~15 GV at the magnetic equator. Note that it should be pointed out that due to the absorption of the particles in the atmosphere at the polar regions, the value of the atmospheric cut-off rigidity at the poles cannot be exactly zero. Thus, the minimum kinetic energy of particles reaching the Earth's surface is about 430 MeV at sea level, and about 300 MeV/n at high-mountain altitude of about 3000a.s.l. which corresponds to the cut-off rigidity about ~1GV (Mishev et al., 2017; Raukunen et al., 2018).

On the other hand, the knowledge of the geomagnetic field (GMF) is needed in order to describe the transport of cosmic rays reaching the Earth. This is because the propagation of cosmic rays is not only influenced by the heliospheric magnetic field carried along by the solar wind plasma, but also by the geomagnetic field. The GMF is assumed to consist by an internal field and by an external one. The dynamics of the Earth's core originates the internal magnetic field and the crustal magnetic field, while the external field is generated in the ionosphere and the magnetosphere. Several models have been developed in order to describe the contribution of the external magnetic field. One of the well-known model is the Tsyganenko model_T89 (Tsyganenko, 1989), which is a semi-empirical best-fit representation for the magnetic field, based on a large number of satellite observations. This model takes into account a complex system of currents consisting of the magnetic field ring current, the magnetotail currents, including the plasma sheet and returns currents, the magnetopause contribution and the average magnetic effect of field-aligned currents. The core field which is the main contributor to the GMF called also main field due to first order forms approximately a dipole with an axis inclined by 11.5° with the rotation axis of the Earth. Multi-pole field expansions exist on this dipole. It changes regularly in along term basis. The current state-of–art representation of Earth's internal magnetic field is the International Geomagnetic Reference Field (IGRF) models generated under the International Association of Geomagnetism and Aeronomy (IAGA) (http://www.iugg.org/associations/iaga.php). The IGRF model is generally revised every 5 years by a group of modelers, reflecting the most accurate calculations available at that time. The latest version of IGRF model is the 13th Generation and was released in December 2019, nevertheless in this study the 12th Generation has been used.

The calculation of cosmic ray particle trajectories arriving at the Earth through its magnetic field has been a subject of study since the epoch of Störmer (1930). The main difficulty related to the fact that there is no analytical solution of the equation of a charged particle moving even in the field of a magnetic dipole (except of the trajectories in the equatorial plane) forced the researchers to develop several techniques of numerical integrations of many individual trajectories to find out the behavior of trajectory groups. Therefore, Smart et al. (2000) presented a review of models of the GMF and the trajectory computations of cosmic rays in this field aiming to determine the cut-off rigidities. In that work, they concluded that the accuracy of the trajectory computations is a function of energy. The accuracy increases as the energy increases. So, the greatest precision achieved for the highest energies. At low energies, due to the fact that the topology of the magnetospheric field dominates the results, the cut-off values can be obtained in comparison with current spacecraft measurements (Kudela and Usoskin, 2004; Kudela et al., 2008; Nevalainen et al., 2013).

In this work, we have determined cosmic-ray cut-off rigidities by the trajectory- tracing method, described in Smart and Shea (2000) and Smart et al. (2000). The orbit of a particle of specified rigidity is traced, by numerical methods, through the geomagnetic field employing the 12th generation of the IGRF in order to determine if the particle is allowed or forbidden for a specific zenith and azimuth at a given location. Applying this procedure we have derived a world grid of vertically incident cosmic ray cut-off rigidities for the three latest epochs**.** For these calculations software from IZMIRAN group was applied which is recently modulated as an online tool (http://tools.izmiran.ru). The geomagnetic cut-off rigidities were calculated in every 5° in latitude and in every 15° in longitude allowing us to compare our results with previous epochs. This precision is reasonable since the gradient for Rc is weaker along the longitude (about 0.1–0.2GV/5°) than the one along the latitude (about 0.8GV/5°). So, a 5X15° grid provides almost equal changes of the cut-off rigidity along the latitude and longitude. Moreover the long-term variation of the vertical cut-off rigidity is discussed.

Extensive and most comprehensive and systematic studies of the magnetospheric effects in cosmic rays, including their long-period changes, were carried out in a series of

works by Smart and Shea (2009). The computed global distribution of the vertical geomagnetic cut- off rigidity for all stations of the Worldwide Neutron Monitor Network for nine five-year eras of 1955–1995 (Shea and Smart, 1975a, 1975b, 2001) drew attention to the uneven changes in the planetary distribution of geomagnetic cut-off rigidity over 20 years from 1955 to 1975, especially on the northern and southern waters of the Atlantic Ocean. A decrease in cut-off rigidity was observed in the southern Atlantic Ocean, while a comparable increase in vertical cut-off rigidity was observed in the northern Atlantic. In a recent work, Smart and Shea (2019) concluded the existence of a continuing decrease in cut-off rigidities along the Southern American region, while there is an increase in the North American east coast region. Over the past three eras covering the period from 2010 to 2020, such calculations for the current network of detectors have not been carried out with an exception for the epoch 2015, which was presented by Smart and Shea (2019). In addition, over the last 20 years, about a third of new Neutron Monitors have been commissioned and a network of multidirectional muon telescopes has been created. For the groups of all these detectors, these maps would be useful to update their geomagnetic cut-off rigidity and the asymptotic acceptance cones calculations.

2. Data and method

A well-known accurate way to determine the geomagnetic cut-off rigidity is the trajectory tracing method, which is described in detail in Shea et al. (1965), Shea and Smart (1967), Humble et al. (1985), Cooke et al. (1991), Smart and Shea (2000), Smart et al. (2000). This method calculates the trajectory of a negatively charged particle moving outward from the Earth from a specific location and direction. This trajectory is the same as that of the positively charged particle of equal rigidity approaching the Earth to arrive at the same position from the same direction. The physical concept of the trajectory-tracing method, which is used in this work, is described in Smart and Shea (2000), Smart et al. (2000) and Gvozdevsky et al. (2019). In this software the cut-off rigidities are calculated by starting with a cosmic ray trajectory at the top of the atmosphere, at the altitude of 20 km above a specific location on Earth, with a vertical incidence, i.e. with zenith angle of 0°. This trajectory is followed until access to the interplanetary medium (at 25 Earth radii) is assured. In this case, the trajectory is named allowed, otherwise the trajectory is called forbidden. These last trajectories are those which intersect the solid Earth, called re-entrant trajectories and those for which no solution can be obtained within a reasonable number of iterations. When the particle cannot leave the magnetosphere it can drift endless, for example, being captured by the radiation belt. In this case the integrating time is limited by a reasonable time of drift, so- called pre-determined time (experimentally this time is about 7–8 s). So, integration is completed in three cases:

1 the particle has moved beyond the magnetosphere,
2 the particle penetrated to a depth less (h + 20) km, is returned to the atmosphere,
3 the integration is completed after the above referred predetermined time and the particle is considered as trapped by the radiation belt.

The trajectory is identified as allowed one in the first case, while in the other cases as forbidden. As a result, a discrete function is formed which takes the values of "0" or "1" for all rigidity values with an integrating step of 0.01 GV.

In order to calculate the effective cut-off rigidity a summation of the allowed and forbidden regions defined by the penumbra region can be carried out. In this case, the effective cut- off rigidity is defined as

$$R_c = R_u - \left[\int_{R_l}^{R_u} dR\right]_{\text{allowed}} \quad (1)$$

where R_u is the upper cut-off rigidity, above which all rigidities are allowed,

R_l is the lower cut-off rigidity, below which all rigidities are forbidden, thus allowing the opacity of the penumbra (Shea et al., 1965).

Beyond the above described summation, an alternative way is a detailed calculation of the effective cut-off rigidity proposed by Dorman et al. (1972). In this calculation (a) the effect of the atmosphere by including additionally coupling functions and (b) different spectral slopes for cosmic ray particles e.g. neutrons and muons, are taken in account. According to this procedure in order to solve the equation that gives the effective cut-off rigidity R_c the spectrum of variations is approximated by a power function and the atmospheric influence through the coupling function, which in a relatively small region of the penumbra is approximated by the power function. Then, by integrating the effective cut-off rigidity is defined as:

$$R_c^{\gamma+n+1} = R_u^{\gamma+n+1}(\gamma + n + 1)\int_{R_l}^{R_u} g(R)\cdot R^{n+\gamma} dR \quad (2)$$

where $g(R)$ is a function of penumbra. In the particular case of the primary spectrum independent of the energy of cosmic rays (white or flat spectrum, i.e. $\gamma = 0$) and by neglecting the atmospheric influence (i.e. $n = 0$), we end up to Eq. (1).

In this work the software used for the calculation of the geomagnetic cut-off rigidity allows to update the IGRF model, whenever a new one is released by the International Association of Geomagnetism and Aeronomy (IAGA). So, the calculated here values are based on the 12th Generation of the International Geomagnetic Reference Field (IGRF 12) which takes into account the secular variation of the geomagnetic field represented by 13 spherical harmonics. Calculating the planetary distribution of the geomagnetic cut-off rigidity, IGRF models for the corresponding era were used, starting, for example, with the IGRF 8 for the

years 2000–2005. The employment of the 12th Generation adopted in December 2014 provides besides the main field for epochs 2010, 2015 and a linear secular variation model for the years 2015–2020. It is added here that during this time period no geomagnetic jerk was occurred that means no significant changes to the projected field coefficients were resulted (Thébault et al., 2015).

3. Results

The worldwide grids of the cut-off rigidities for vertical directions of arrival of the cosmic ray particles at the altitude of 20 km above the surface of the international reference ellipsoid, have been computed. These grids of the vertical cut-off rigidity cover the last decade from 2010 until today. The average annual values of the effective cut-off rigidities are calculated applying the trajectory-tracing method using the 12th Generation of the IGRF 12. A five-degree in latitude and fifteen degrees in longitude tabulation of the calculated effective cut-off rigidities for the epoch 2010 is given in Table 1. The calculated values for the epoch 2015 are presented in Table 2, while Table 3 is referred to the current year 2020.

The graphical representation of the calculated geomagnetic cut-off rigidities produced by our method for the years 2010, 2015 and 2020 are given through contour plots appeared in Fig. 1a–c respectively. Note that these epochs cover the start of the solar cycle 24, the maximum and the end of this cycle and no significant differences between all these calculated cut-off rigidities are observed. In order to present the variation of the cut-off rigidity during the last decade contour plots showing the differences in magnitude of the change in calculated cut-off rigidity between the present year 2020, the year 2015 and the year 2010 are created and presented in Fig. 2a and b respectively. Moreover, a contour plot presenting the differences in cut-off rigidities between the year 2020 and 2015 is given in Fig. 2c. As we can see from all above plots the majority of the cut-off rigidities exhibit almost no changes except minor changes within 0.1GV. This is expected since the 2015 coefficients with the corresponding approximation of the secular variation are used in all cases. Some differences that are observed in two well defined geographic area limited between 35–50° South and 75–130° West and its eastern "tail are in accordance with the North Atlantic anomaly (Gvozdevsky et al., 2019; Smart and Shea, 2019).

Furthermore, it is important to note that the calculated values of the cut-off rigidity for the year 2015 presented in this work are in agreement with the corresponding ones presented by Smart and Shea (2019). A comparison between these two tables is presented in Fig. 3. As we can conclude the great majority of the calculated values presented in this work are consistent with Smart and Shea (2019) calculations. Deviations within 0.1 GeV are at minor significance. While certain discrepancies greater than 0.5 GeV that are observed in a narrow eastern area in the middle latitude locations in two well-defined zones, from 45° to 10° North and 25° to 50° South respectively, are observed. These differences might be explained by the penumbra and possibly deviations between the used software. A more detailed analysis might be useful in the future. In order to present the cut-off rigidity values for the present epoch of 2020 in a more adequately visualized form, a world map displaying the *iso*-rigidity curves is given in Fig. 4.

4. Discussion and conclusions

The present work could be considered as an extension in time of the previous published works referred to the worldwide grid by Shea and Smart (1983) and Smart and Shea (1997, 2006, 2007, 2008, 2019) covering the last decade and updating the worldwide grid of the vertical cut-off rigidities for the current epoch of 2020. It is important to note that this time period from 2010 to 2020 covers the current solar cycle 24 that is characterized by low geomagnetic activities in comparison with the previous solar cycle 23 (Alexakis and Mavromichalaki, 2019)

As we can conclude from this study there are minor changes in the effective cut-off rigidities over the world during the last decade. Small observed decreases in these values are consistent with the region of the South Atlantic anomaly (Gvozdevsky et al., 2019). The results of this work could be a reference for evaluating the effects associated with the latitude and longitude distribution of the geomagnetic rigidity. For instance, tabulations, such as these are an useful tool for estimating the radiation dose in aviation due to cosmic radiation. The aircraft radiation dose calculations by different models, such as CARI-6 (Friedberg et al., 1999), EPCARD (Schraube et al., 2000) and PCAIRE (Lewis et al., 2005) use geomagnetic cut-off rigidities for various epochs to calculate radiation dose along worldwide flight paths. Recently, the new product DYASTIMA/DYASTIMA-R of the ESA SSA Space Radiation Expert Center provided by the Cosmic **R**ay Group of the National and Kapodistrian University of Athens calculates also the radiation doses at different altitudes and different particles using cut-off rigidities (Tezari et al., 2020).

Nevertheless, the development and provision of worldwide grids of cut-off rigidities for vertical directions of the arrival of the cosmic ray particles at the altitude of 20 km above the surface of the international reference ellipsoid has been a subject of interest by the scientific community since they can be useful for fundamental research and applications as well. It has become recognized that there is a general need for useful geomagnetic cut-off rigidity at a specific location. As an example, Zreda (2012) has developed a web based procedure (http://cosmos.hwr.arizona.edu/Util/rigidity.php) where the user enters a geographic coordinate and receives a geomagnetic cut-off for that location. Recently, another tool which provides calculations of cut-off rigidities until the year 2050, is developed by IZMIRAN group (http://tools.izmiran.ru)

Table 1
Effective Vertical Cut-off Rigidities (in GV) for the epoch 2010.

	World Grid IGRF 2010												Geographic East Longitude												
	−180	−165	−150	−135	−120	−105	−90	−75	−60	−45	−30	−15	0	15	30	45	60	75	90	105	120	135	150	165	180
Lat																									
90	0.00	0.00	0.00	0.00	0.00	0.00	0.00	0.00	0.00	0.00	0.00	0.00	0.00	0.00	0.00	0.00	0.00	0.00	0.00	0.00	0.00	0.00	0.00	0.00	0.00
85	0.00	0.00	0.00	0.00	0.00	0.00	0.00	0.00	0.00	0.00	0.00	0.00	0.00	0.00	0.00	0.00	0.00	0.00	0.00	0.00	0.00	0.00	0.00	0.00	0.00
80	0.04	0.02	0.00	0.00	0.00	0.00	0.00	0.00	0.00	0.00	0.00	0.00	0.02	0.03	0.05	0.05	0.06	0.07	0.07	0.07	0.07	0.07	0.06	0.05	0.04
75	0.15	0.11	0.07	0.03	0.00	0.00	0.00	0.00	0.00	0.01	0.04	0.07	0.09	0.12	0.14	0.16	0.17	0.18	0.18	0.19	0.20	0.21	0.20	0.18	0.15
70	0.39	0.29	0.20	0.12	0.06	0.03	0.01	0.02	0.04	0.08	0.13	0.19	0.25	0.31	0.34	0.37	0.39	0.40	0.42	0.44	0.47	0.48	0.49	0.46	0.39
65	0.83	0.66	0.46	0.30	0.17	0.10	0.08	0.09	0.13	0.22	0.34	0.47	0.58	0.66	0.72	0.75	0.76	0.78	0.82	0.87	0.92	0.99	1.01	0.96	0.83
60	1.57	1.26	0.94	0.63	0.40	0.26	0.21	0.23	0.33	0.51	0.73	0.97	1.13	1.27	1.32	1.36	1.38	1.43	1.47	1.56	1.66	1.78	1.85	1.77	1.57
55	2.64	2.16	1.65	1.18	0.79	0.55	0.45	0.48	0.68	1.00	1.40	1.78	2.02	2.15	2.22	2.25	2.32	2.36	2.45	2.59	2.77	2.96	3.04	2.95	2.64
50	4.00	3.29	2.67	2.01	1.43	1.01	0.85	0.92	1.26	1.82	2.50	2.96	3.27	3.40	3.46	3.49	3.58	3.69	3.84	4.03	4.26	4.56	4.65	4.49	4.00
45	5.34	4.74	4.02	3.09	2.32	1.73	1.45	1.53	2.05	2.95	4.00	4.62	4.90	5.00	5.03	5.10	5.22	5.41	5.56	5.78	6.03	6.29	6.32	5.92	5.34
40	7.55	6.32	5.38	4.54	3.51	2.68	2.25	2.42	3.17	4.53	5.63	6.61	7.09	7.14	7.04	7.06	7.32	7.69	8.05	8.39	8.88	9.23	9.17	8.56	7.55
35	9.35	8.82	7.54	5.92	4.96	3.92	3.29	3.52	4.60	6.31	8.66	9.53	9.74	9.63	9.74	10.00	10.50	10.89	11.20	11.05	11.28	11.44	11.09	10.25	9.35
30	11.51	10.35	9.58	8.41	6.56	5.20	4.28	4.58	6.26	9.20	10.85	11.34	11.59	11.66	11.74	12.09	12.61	13.10	13.61	13.87	13.86	13.65	13.17	12.48	11.51
25	12.80	12.13	11.40	10.43	9.03	7.17	5.89	6.25	8.70	11.22	12.35	12.98	13.34	13.59	13.82	14.15	14.61	15.07	15.36	15.39	15.20	14.81	14.21	13.51	12.80
20	13.65	13.06	12.46	11.71	10.52	8.26	7.06	7.55	10.62	12.35	13.26	13.85	14.28	14.61	14.89	15.25	15.76	16.26	16.53	16.48	16.17	15.66	15.00	14.31	13.65
15	14.32	13.79	13.28	12.66	11.68	10.17	9.11	10.00	11.92	12.98	13.72	14.25	14.70	15.11	15.48	15.93	16.50	17.02	17.28	17.19	16.80	16.23	15.57	14.91	14.32
10	14.82	14.35	13.90	13.38	12.66	11.67	10.97	11.57	12.50	13.28	13.82	14.25	14.71	15.18	15.64	16.18	16.82	17.37	17.64	17.53	17.11	16.53	15.91	15.34	14.82
5	15.13	14.72	14.30	13.85	13.31	12.59	12.10	12.24	12.77	13.30	13.61	13.90	14.33	14.83	15.38	16.03	16.74	17.32	17.60	17.50	17.09	16.55	16.01	15.55	15.13
0	15.20	14.86	14.49	14.09	13.64	13.11	12.63	12.52	12.81	13.06	13.12	13.24	13.60	14.11	14.73	15.49	16.26	16.87	17.16	17.10	16.74	16.27	15.85	15.52	15.20
−5	15.01	14.76	14.46	14.12	13.73	13.27	12.80	12.58	12.64	12.63	12.42	12.36	12.60	13.08	13.77	14.61	15.42	16.02	16.32	16.32	16.05	15.68	15.39	15.20	15.01
−10	14.52	14.39	14.20	13.94	13.62	13.22	12.76	12.44	12.30	12.01	11.53	11.22	11.38	11.85	12.57	13.45	14.25	14.80	15.09	15.15	14.97	14.71	14.55	14.53	14.52
−15	13.65	13.73	13.69	13.55	13.32	12.99	12.55	12.13	11.80	11.28	10.53	9.85	9.96	10.35	11.13	12.02	12.67	13.19	13.42	13.53	13.45	13.29	13.30	13.45	13.65
−20	12.32	12.70	12.91	12.95	12.85	12.59	12.18	11.67	11.17	10.31	9.25	8.43	8.22	8.65	9.29	9.99	10.50	10.79	10.93	11.11	11.04	10.52	10.63	11.63	12.32
−25	9.70	10.62	11.56	12.12	12.19	12.04	11.68	11.09	10.31	9.29	7.96	7.01	6.85	7.13	7.65	8.11	8.18	7.93	7.65	7.70	7.81	7.95	8.48	9.33	9.70
−30	7.62	8.95	8.87	10.49	11.32	11.35	11.06	10.32	9.43	8.15	6.73	5.99	5.50	5.56	5.82	5.84	5.61	5.37	5.25	5.19	5.27	5.45	5.82	6.48	7.62
−35	5.37	6.25	7.64	8.06	9.69	10.49	10.19	9.49	8.41	6.94	5.88	5.03	4.40	4.24	4.30	4.30	4.11	3.80	3.44	3.39	3.43	3.65	4.14	4.78	5.37
−40	3.95	4.54	5.32	6.50	7.95	9.35	9.21	8.53	7.35	6.26	5.16	4.08	3.58	3.36	3.35	3.19	2.78	2.46	2.15	2.06	2.10	2.23	2.61	3.17	3.95
−45	2.56	3.14	4.10	4.78	5.88	7.54	8.15	7.67	6.73	5.48	4.16	3.36	2.91	2.69	2.47	2.24	1.89	1.53	1.26	1.11	1.13	1.24	1.52	1.97	2.56
−50	1.57	2.16	2.79	3.65	4.43	5.24	6.19	6.20	5.31	4.27	3.40	2.75	2.34	2.08	1.83	1.56	1.22	0.91	0.67	0.55	0.54	0.61	0.80	1.11	1.57
−55	0.89	1.32	1.87	2.50	3.22	4.02	4.46	4.47	4.08	3.45	2.85	2.25	1.86	1.58	1.33	1.06	0.78	0.51	0.33	0.24	0.22	0.26	0.37	0.57	0.89
−60	0.46	0.75	1.13	1.61	2.19	2.76	3.30	3.45	3.21	2.66	2.18	1.76	1.44	1.19	0.93	0.69	0.46	0.28	0.15	0.09	0.07	0.08	0.14	0.26	0.46
−65	0.22	0.40	0.67	1.01	1.42	1.82	2.17	2.32	2.21	1.95	1.60	1.32	1.06	0.85	0.64	0.44	0.27	0.14	0.06	0.01	0.00	0.00	0.04	0.10	0.22
−70	0.10	0.21	0.38	0.59	0.85	1.11	1.34	1.45	1.43	1.31	1.12	0.92	0.74	0.57	0.41	0.28	0.15	0.07	0.02	0.00	0.00	0.00	0.00	0.03	0.10
−75	0.05	0.11	0.20	0.33	0.48	0.63	0.77	0.85	0.86	0.81	0.72	0.60	0.49	0.36	0.26	0.17	0.09	0.04	0.00	0.00	0.00	0.00	0.00	0.00	0.05
−80	0.03	0.06	0.12	0.18	0.26	0.34	0.40	0.44	0.46	0.44	0.40	0.35	0.29	0.22	0.16	0.10	0.06	0.03	0.00	0.00	0.00	0.00	0.00	0.00	0.03
−85	0.04	0.06	0.08	0.11	0.14	0.16	0.19	0.21	0.21	0.21	0.20	0.18	0.15	0.13	0.10	0.08	0.06	0.04	0.03	0.02	0.01	0.01	0.02	0.03	0.04
−90	0.08	0.08	0.08	0.08	0.08	0.08	0.08	0.08	0.08	0.08	0.08	0.08	0.08	0.08	0.08	0.08	0.08	0.08	0.08	0.08	0.08	0.08	0.08	0.08	0.08

Table 2
Effective Vertical Cut-off Rigidities (in GV) for the epoch 2015.

	World Grid IGRF 2015												Geographic East Longitude												
	−180	−165	−150	−135	−120	−105	−90	−75	−60	−45	−30	−15	0	15	30	45	60	75	90	105	120	135	150	165	180
Lat																									
90	0.00	0.00	0.00	0.00	0.00	0.00	0.00	0.00	0.00	0.00	0.00	0.00	0.00	0.00	0.00	0.00	0.00	0.00	0.00	0.00	0.00	0.00	0.00	0.00	0.00
85	0.00	0.00	0.00	0.00	0.00	0.00	0.00	0.00	0.00	0.00	0.00	0.00	0.00	0.00	0.00	0.00	0.00	0.00	0.00	0.00	0.00	0.00	0.00	0.00	0.00
80	0.04	0.02	0.00	0.00	0.00	0.00	0.00	0.00	0.00	0.00	0.00	0.00	0.02	0.03	0.04	0.05	0.05	0.06	0.06	0.06	0.07	0.06	0.06	0.05	0.04
75	0.14	0.10	0.07	0.03	0.00	0.00	0.00	0.00	0.00	0.01	0.04	0.07	0.09	0.12	0.14	0.15	0.16	0.16	0.17	0.18	0.19	0.19	0.19	0.17	0.14
70	0.37	0.29	0.19	0.12	0.06	0.03	0.02	0.02	0.05	0.08	0.14	0.20	0.25	0.30	0.34	0.36	0.37	0.38	0.40	0.42	0.45	0.46	0.47	0.44	0.37
65	0.81	0.64	0.46	0.29	0.18	0.11	0.09	0.10	0.14	0.23	0.35	0.48	0.58	0.65	0.70	0.72	0.75	0.76	0.79	0.83	0.89	0.94	0.97	0.92	0.81
60	1.53	1.25	0.91	0.63	0.41	0.27	0.22	0.24	0.35	0.53	0.76	0.96	1.15	1.26	1.31	1.33	1.35	1.38	1.41	1.49	1.63	1.74	1.79	1.74	1.53
55	2.59	2.13	1.63	1.17	0.81	0.57	0.47	0.52	0.71	1.06	1.47	1.82	2.04	2.13	2.19	2.22	2.27	2.29	2.36	2.51	2.70	2.88	3.00	2.88	2.59
50	3.95	3.24	2.66	2.00	1.43	1.04	0.87	0.95	1.30	1.89	2.58	3.00	3.28	3.39	3.41	3.43	3.48	3.60	3.70	3.91	4.19	4.45	4.60	4.43	3.95
45	5.32	4.70	3.99	3.09	2.32	1.75	1.48	1.60	2.17	3.07	4.11	4.67	4.94	4.99	4.98	5.02	5.14	5.31	5.46	5.65	5.94	6.21	6.25	5.86	5.32
40	7.49	6.25	5.33	4.51	3.48	2.69	2.31	2.48	3.34	4.72	5.77	6.74	7.19	7.16	6.98	6.96	7.21	7.51	7.81	8.17	8.74	9.12	9.09	8.51	7.49
35	9.34	8.74	7.44	5.86	4.89	3.87	3.36	3.62	4.76	6.61	8.88	9.64	9.78	9.66	9.70	9.93	10.40	10.73	10.89	10.95	11.16	11.38	11.04	10.21	9.34
30	11.47	10.28	9.49	8.31	6.50	5.18	4.35	4.77	6.62	9.54	10.91	11.45	11.65	11.68	11.73	12.04	12.52	12.91	13.39	13.76	13.79	13.61	13.14	12.45	11.47
25	12.76	12.06	11.30	10.32	8.91	7.09	5.93	6.48	9.11	11.39	12.46	13.06	13.39	13.62	13.82	14.14	14.57	15.01	15.28	15.31	15.15	14.79	14.20	13.49	12.76
20	13.60	12.98	12.36	11.59	10.32	8.13	6.81	7.57	10.98	12.46	13.33	13.90	14.32	14.63	14.90	15.25	15.75	16.22	16.48	16.43	16.14	15.65	14.99	14.29	13.60
15	14.28	13.72	13.18	12.54	11.53	10.06	9.22	10.27	12.03	13.05	13.76	14.28	14.73	15.13	15.49	15.94	16.51	17.01	17.26	17.17	16.79	16.23	15.56	14.89	14.28
10	14.78	14.28	13.80	13.26	12.53	11.57	10.99	11.67	12.56	13.32	13.84	14.27	14.73	15.19	15.65	16.21	16.85	17.40	17.65	17.53	17.11	16.53	15.90	15.31	14.78
5	15.08	14.65	14.21	13.74	13.19	12.51	12.07	12.25	12.79	13.29	13.59	13.89	14.33	14.84	15.40	16.07	16.79	17.37	17.64	17.52	17.10	16.55	16.00	15.52	15.08
0	15.16	14.80	14.41	13.99	13.53	13.01	12.55	12.48	12.79	13.02	13.07	13.20	13.58	14.10	14.76	15.54	16.33	16.94	17.22	17.14	16.77	16.28	15.84	15.48	15.16
−5	14.97	14.71	14.39	14.03	13.63	13.16	12.70	12.51	12.58	12.54	12.32	12.29	12.56	13.07	13.80	14.67	15.51	16.12	16.41	16.39	16.09	15.68	15.37	15.16	14.97
−10	14.48	14.34	14.13	13.86	13.52	13.11	12.65	12.34	12.19	11.89	11.39	11.12	11.32	11.83	12.60	13.52	14.34	14.91	15.20	15.24	15.03	14.71	14.53	14.50	14.48
−15	13.62	13.69	13.63	13.48	13.22	12.87	12.43	12.01	11.67	11.12	10.37	9.73	9.88	10.32	11.16	12.07	12.78	13.31	13.55	13.66	13.52	13.31	13.28	13.41	13.62
−20	12.29	12.67	12.86	12.88	12.75	12.48	12.04	11.53	11.00	10.11	9.04	8.26	8.14	8.63	9.31	10.04	10.56	10.80	11.13	11.29	11.19	10.51	10.62	11.62	12.29
−25	9.66	10.63	11.56	12.06	12.10	11.93	11.54	10.91	10.12	9.06	7.75	6.85	6.73	7.12	7.67	8.14	8.27	8.01	7.80	7.89	7.87	7.91	8.48	9.28	9.66
−30	7.61	8.96	8.72	10.49	11.24	11.23	10.90	10.14	9.22	7.91	6.54	5.82	5.43	5.54	5.83	5.88	5.63	5.46	5.34	5.30	5.36	5.47	5.82	6.46	7.61
−35	5.39	6.26	7.65	8.04	9.69	10.38	10.03	9.30	8.17	6.72	5.67	4.87	4.32	4.21	4.29	4.30	4.12	3.85	3.52	3.48	3.50	3.70	4.16	4.79	5.39
−40	3.97	4.53	5.32	6.51	7.89	9.25	9.04	8.30	7.09	6.02	4.95	3.96	3.51	3.34	3.36	3.25	3.01	3.00	3.00	2.13	2.17	3.00	3.00	3.21	3.97
−45	3.00	3.22	4.08	4.76	5.87	7.47	8.01	7.49	6.56	5.22	4.00	3.28	3.05	2.68	2.46	2.24	2.03	2.00	2.00	1.16	1.16	2.00	2.00	2.06	3.00
−50	2.00	2.18	3.04	3.64	4.43	5.18	6.05	5.98	5.07	4.13	3.30	2.66	2.30	2.07	1.81	1.54	1.21	1.00	1.00	0.57	0.55	1.00	1.00	1.12	2.00
−55	1.00	1.31	2.02	3.00	3.24	3.96	4.38	4.36	3.96	3.35	2.76	2.19	1.84	1.56	1.31	1.05	0.76	0.51	0.34	0.24	0.22	0.26	0.37	0.58	1.00
−60	0.47	0.76	1.14	2.00	2.17	3.00	3.24	3.40	3.18	2.55	2.12	1.72	1.41	1.16	0.92	0.68	0.46	0.27	0.15	0.09	0.07	0.09	0.14	0.26	0.47
−65	0.22	0.41	0.67	1.02	1.41	2.00	2.12	2.27	2.16	2.01	1.54	1.27	1.02	0.82	0.63	0.43	0.27	0.14	0.06	0.01	0.00	0.00	0.04	0.11	0.22
−70	0.10	0.21	0.38	0.58	0.84	1.09	1.31	1.42	1.39	1.28	1.08	0.89	0.72	0.55	0.41	0.27	0.15	0.07	0.01	0.00	0.00	0.00	0.00	0.03	0.10
−75	0.05	0.11	0.20	0.33	0.47	0.62	0.75	0.82	0.83	0.79	0.69	0.58	0.47	0.36	0.25	0.16	0.09	0.04	0.00	0.00	0.00	0.00	0.00	0.00	0.05
−80	0.03	0.07	0.12	0.18	0.26	0.33	0.39	0.43	0.45	0.44	0.39	0.35	0.28	0.22	0.15	0.10	0.06	0.03	0.00	0.00	0.00	0.00	0.00	0.00	0.03
−85	0.04	0.06	0.08	0.10	0.13	0.16	0.18	0.20	0.21	0.20	0.19	0.18	0.15	0.13	0.10	0.08	0.06	0.04	0.02	0.02	0.01	0.01	0.02	0.02	0.04
−90	0.08	0.08	0.08	0.08	0.08	0.08	0.08	0.08	0.08	0.08	0.08	0.08	0.08	0.08	0.08	0.08	0.08	0.08	0.08	0.08	0.07	0.08	0.08	0.08	0.08

Table 3
Effective Vertical Cut-off Rigidities (in GV) for the epoch 2020.

	World Grid IGRF 2020												Geographic East Longitude												
	−180	−165	−150	−135	−120	−105	−90	−75	−60	−45	−30	−15	0	15	30	45	60	75	90	105	120	135	150	165	180
Lat																									
90	0.00	0.00	0.00	0.00	0.00	0.00	0.00	0.00	0.00	0.00	0.00	0.00	0.00	0.00	0.00	0.00	0.00	0.00	0.00	0.00	0.00	0.00	0.00	0.00	0.00
85	0.00	0.00	0.00	0.00	0.00	0.00	0.00	0.00	0.00	0.00	0.00	0.00	0.00	0.00	0.00	0.00	0.00	0.00	0.00	0.00	0.00	0.00	0.00	0.00	0.00
80	0.03	0.02	0.00	0.00	0.00	0.00	0.00	0.00	0.00	0.00	0.00	0.00	0.02	0.03	0.04	0.04	0.05	0.06	0.06	0.06	0.06	0.06	0.05	0.05	0.03
75	0.13	0.10	0.06	0.03	0.00	0.00	0.00	0.00	0.00	0.02	0.04	0.07	0.09	0.11	0.13	0.14	0.15	0.16	0.16	0.17	0.18	0.18	0.18	0.16	0.13
70	0.36	0.28	0.19	0.11	0.06	0.03	0.02	0.03	0.05	0.09	0.14	0.20	0.26	0.30	0.33	0.35	0.35	0.36	0.38	0.40	0.42	0.45	0.45	0.42	0.36
65	0.79	0.62	0.45	0.29	0.18	0.12	0.09	0.11	0.16	0.25	0.36	0.49	0.59	0.65	0.69	0.71	0.72	0.73	0.76	0.79	0.86	0.91	0.93	0.90	0.79
60	1.49	1.21	0.91	0.62	0.41	0.28	0.24	0.26	0.37	0.55	0.78	0.98	1.15	1.26	1.29	1.31	1.33	1.34	1.38	1.44	1.59	1.69	1.75	1.68	1.49
55	2.54	2.10	1.62	1.16	0.81	0.58	0.50	0.54	0.76	1.09	1.53	1.87	2.07	2.14	2.17	2.18	2.20	2.24	2.29	2.44	2.65	2.84	2.95	2.84	2.54
50	3.93	3.22	2.63	2.01	1.43	1.07	0.92	1.01	1.37	1.98	2.65	3.08	3.33	3.43	3.40	3.40	3.42	3.52	3.62	3.81	4.15	4.38	4.56	4.36	3.93
45	5.30	4.66	3.97	3.08	2.33	1.77	1.52	1.70	2.29	3.21	4.22	4.76	4.97	5.02	4.99	4.97	5.10	5.20	5.35	5.56	5.85	6.13	6.21	5.83	5.30
40	7.42	6.20	5.29	4.49	3.48	2.72	2.36	2.60	3.59	4.84	5.94	6.91	7.25	7.17	6.95	6.91	7.10	7.35	7.59	7.95	8.62	9.09	9.04	8.49	7.42
35	9.32	8.65	7.33	5.81	4.84	3.83	3.41	3.72	4.97	6.94	9.08	9.75	9.80	9.67	9.67	9.88	10.30	10.58	10.83	10.95	11.06	11.34	10.99	10.17	9.32
30	11.42	10.19	9.28	8.17	6.42	5.13	4.41	4.96	7.06	9.81	11.00	11.56	11.72	11.71	11.73	12.01	12.44	12.74	13.16	13.65	13.73	13.59	13.13	12.42	11.42
25	12.70	11.97	11.18	10.19	8.73	7.00	5.99	6.77	9.31	11.55	12.56	13.14	13.46	13.65	13.83	14.13	14.55	14.95	15.20	15.24	15.11	14.77	14.19	13.47	12.70
20	13.56	12.90	12.24	11.45	10.11	8.02	6.65	7.79	11.22	12.56	13.40	13.96	14.36	14.66	14.91	15.25	15.74	16.19	16.43	16.38	16.12	15.65	14.99	14.27	13.56
15	14.23	13.64	13.07	12.41	11.39	9.95	9.31	10.50	12.13	13.12	13.81	14.33	14.77	15.15	15.51	15.96	16.52	17.01	17.24	17.14	16.78	16.23	15.56	14.87	14.23
10	14.73	14.21	13.70	13.15	12.40	11.49	11.00	11.73	12.61	13.35	13.86	14.29	14.75	15.21	15.67	16.24	16.89	17.42	17.66	17.53	17.11	16.53	15.89	15.29	14.73
5	15.04	14.58	14.12	13.64	13.08	12.42	12.04	12.25	12.80	13.29	13.58	13.89	14.33	14.84	15.42	16.11	16.84	17.42	17.67	17.54	17.12	16.55	15.99	15.50	15.04
0	15.12	14.74	14.33	13.90	13.43	12.91	12.48	12.45	12.76	12.98	13.02	13.17	13.56	14.10	14.78	15.60	16.40	17.01	17.28	17.19	16.79	16.28	15.82	15.46	15.12
−5	14.93	14.66	14.32	13.94	13.53	13.06	12.61	12.44	12.52	12.47	12.24	12.21	12.52	13.06	13.83	14.74	15.59	16.20	16.50	16.45	16.12	15.68	15.34	15.14	14.93
−10	14.45	14.30	14.07	13.78	13.43	13.00	12.55	12.25	12.10	11.79	11.27	11.03	11.25	11.82	12.63	13.59	14.43	15.01	15.31	15.33	15.07	14.71	14.50	14.47	14.45
−15	13.60	13.65	13.58	13.41	13.14	12.77	12.31	11.90	11.55	10.97	10.14	9.59	9.80	10.31	11.19	12.11	12.87	13.42	13.69	13.78	13.58	13.30	13.25	13.38	13.60
−20	12.27	12.66	12.82	12.82	12.66	12.37	11.92	11.40	10.82	9.92	8.86	8.11	8.06	8.60	9.35	10.10	10.64	11.02	11.34	11.49	11.04	10.50	10.58	11.61	12.27
−25	9.63	10.67	11.58	12.00	12.01	11.82	11.41	10.74	9.94	8.83	7.58	6.72	6.66	7.11	7.70	8.17	8.31	8.12	8.02	8.11	8.02	7.94	8.46	9.26	9.63
−30	7.63	8.99	8.75	10.52	11.16	11.13	10.73	9.96	9.02	7.70	6.35	5.68	5.35	5.55	5.84	5.87	5.69	5.51	5.44	5.41	5.45	5.50	5.83	6.46	7.63
−35	5.39	6.27	7.69	7.95	9.68	10.28	9.87	9.13	7.96	6.52	5.56	4.73	4.26	4.20	4.28	4.30	4.14	3.90	3.62	3.57	3.59	3.73	4.17	4.82	5.39
−40	3.99	4.49	5.34	6.51	7.85	9.14	8.88	8.12	6.87	5.88	4.75	3.86	3.45	3.34	3.35	3.24	3.01	3.00	3.00	3.00	3.00	3.00	3.00	3.21	3.99
−45	3.00	3.25	4.09	4.76	5.86	7.43	7.88	7.34	6.41	5.01	3.88	3.20	2.78	2.63	2.44	2.24	2.04	2.00	2.00	2.00	2.00	2.00	2.00	2.07	3.00
−50	2.00	2.18	3.03	3.67	4.42	5.13	5.90	5.76	4.90	3.99	3.21	2.65	2.23	2.05	1.80	1.52	1.21	1.00	1.00	1.00	1.00	1.00	1.00	1.15	2.00
−55	1.00	1.32	2.03	3.00	3.25	3.92	4.31	4.27	3.86	3.24	2.65	2.14	1.81	1.53	1.29	1.05	0.75	0.51	0.33	0.25	0.23	0.27	0.38	0.59	1.00
−60	0.48	0.77	1.14	2.00	2.17	3.00	3.17	3.32	3.07	2.48	2.04	1.65	1.36	1.13	0.90	0.68	0.45	0.27	0.15	0.09	0.07	0.09	0.15	0.27	0.48
−65	0.23	0.42	0.68	1.02	1.40	2.00	2.09	2.23	2.13	1.80	1.50	1.22	1.00	0.80	0.61	0.42	0.26	0.13	0.06	0.01	0.00	0.00	0.04	0.11	0.23
−70	0.10	0.21	0.37	0.59	0.83	1.07	1.28	1.37	1.34	1.23	1.04	0.88	0.70	0.55	0.40	0.26	0.15	0.06	0.01	0.00	0.00	0.00	0.00	0.03	0.10
−75	0.05	0.11	0.20	0.33	0.47	0.62	0.73	0.81	0.81	0.75	0.67	0.57	0.45	0.35	0.25	0.16	0.08	0.03	0.00	0.00	0.00	0.00	0.00	0.00	0.05
−80	0.03	0.07	0.12	0.18	0.25	0.32	0.38	0.42	0.44	0.42	0.38	0.33	0.27	0.21	0.15	0.10	0.06	0.02	0.00	0.00	0.00	0.00	0.00	0.00	0.03
−85	0.04	0.06	0.08	0.10	0.13	0.16	0.18	0.19	0.20	0.20	0.19	0.17	0.15	0.12	0.10	0.07	0.05	0.04	0.02	0.01	0.00	0.00	0.01	0.02	0.04
−90	0.07	0.07	0.07	0.07	0.07	0.07	0.07	0.07	0.07	0.08	0.08	0.07	0.07	0.07	0.07	0.07	0.07	0.07	0.07	0.08	0.07	0.07	0.07	0.07	0.07

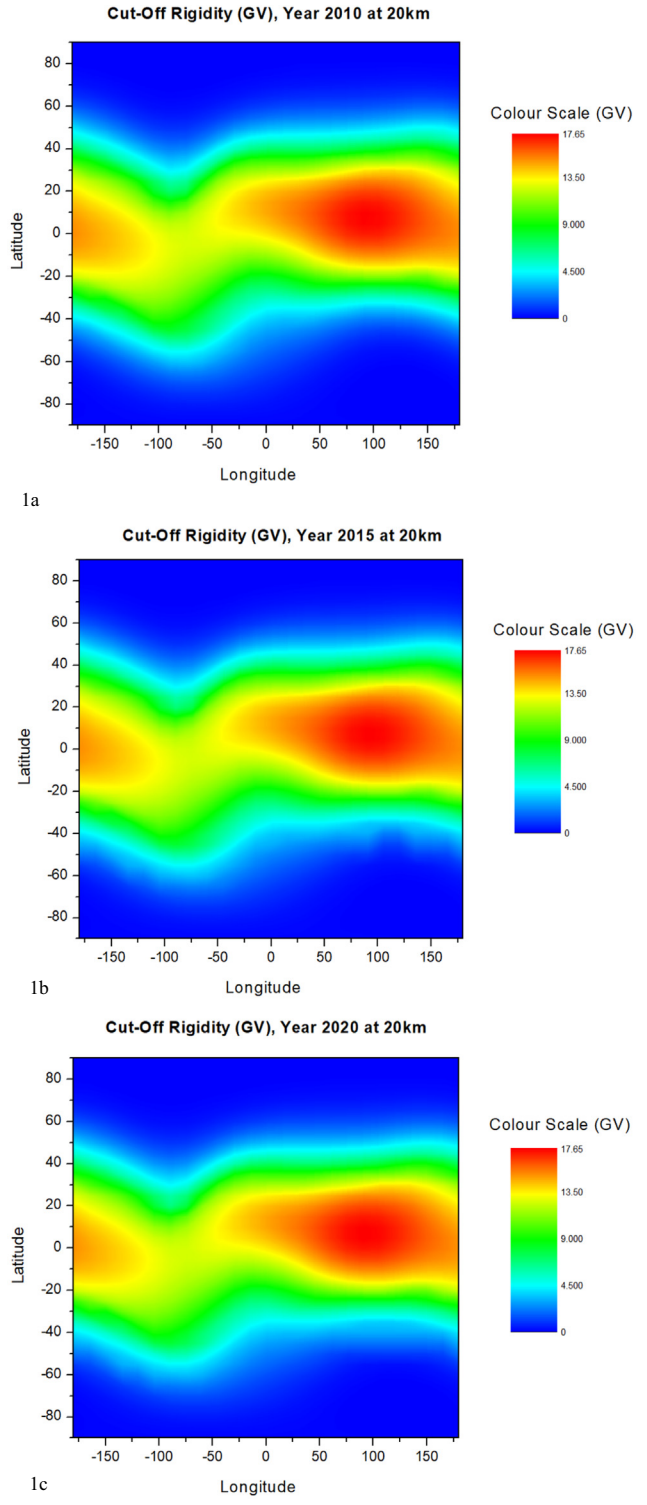

Fig. 1. Contour plot of the geomagnetic cut-off rigidity (a) for the year 2010 (upper panel), (b) for the year 2015 (middle panel) and (c) for the year 2020 (lower panel).

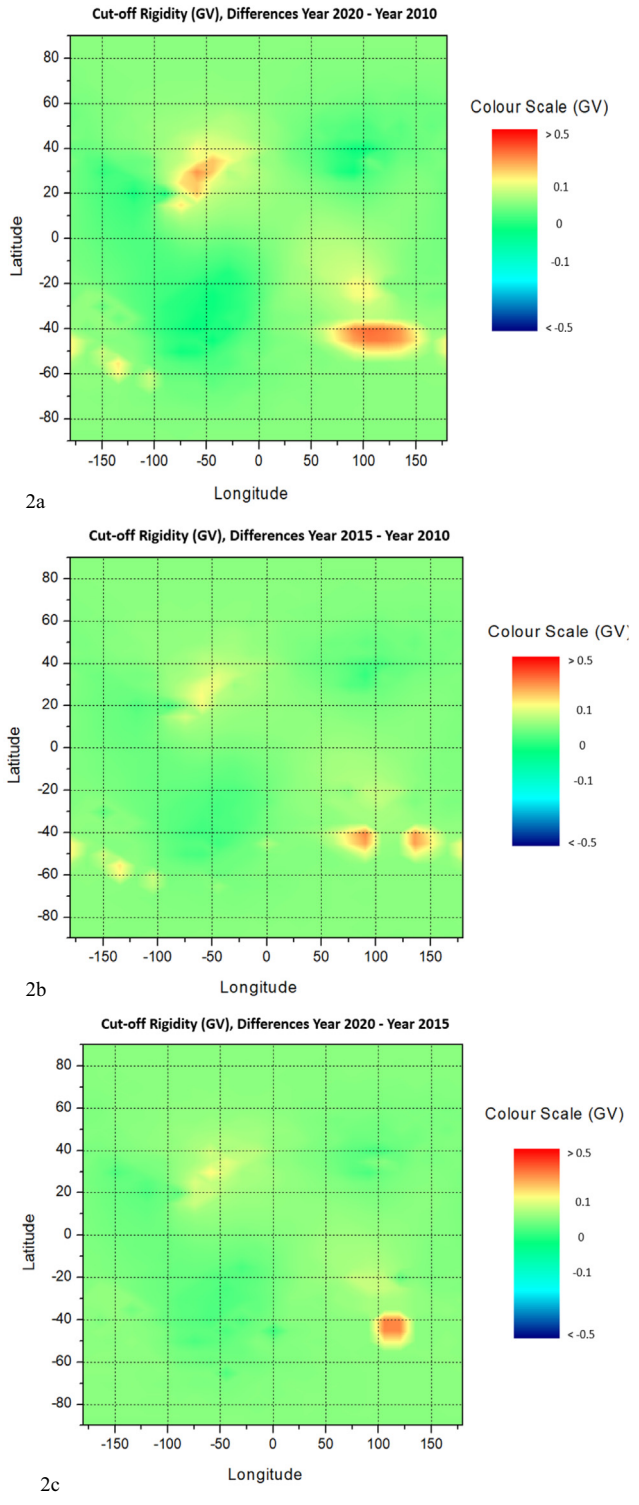

Fig. 2. Contour plot showing the differences in the calculated cut-off rigidities between (a) years 2020 and 2010, (b) years 2015 and 2010 and (c) years 2020 and year 2015.

The main conclusions of this work can be briefly presented below:

(a) This work ensures that the calculation of the world-wide grids of the cut-off rigidity for vertical directions of arrival of the cosmic ray particles at the altitude of 20 km above the surface of the international reference ellipsoid for the current epoch of 2020, is noteworthy. As we can conclude the calculated values of the vertical cut-off rigidity during the last decade show only minor changes.

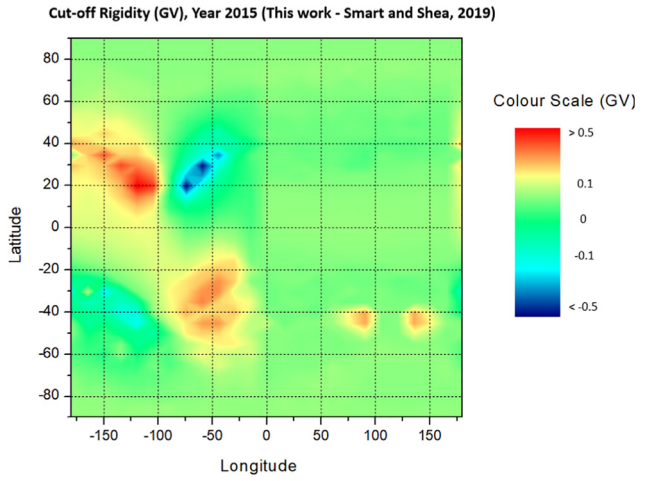

Fig. 3. Contour plot showing the differences between the cut-off rigidity calculated in this work and in Shea and Smart (2019) for the epoch of 2015.

(b) Cosmic ray cut-off rigidity tables and maps over the world concerning the epochs 2010, 2015 and 2020 covering the last decade, have been computed in order to investigate their long-term variation. Minor changes observed in Fig. 2 during these years, are consistent with the North Atlantic anomaly, although it needs a longer time period for study (Gvozdevsky et al., 2019).

(c) From our analysis it is resulted that the calculated values of cut-off rigidity during the year 2015 are in a good agreement with those ones presented by Shea and Smart (2019) for the same year. It means that our calculation procedure for the calculations of the years 2010 till the year 2020 follows well the international standards.

Summarizing we can say that no significant variation in the threshold of the effective geomagnetic rigidity during the last decade, was occurred. However the estimation of the worldwide cut-off rigidity every five-year is important for the neutron monitor network measurements, in particular for the neutron monitor stations located near and at the periphery of North and South Atlantic anomaly (Gvozdevsky et al., 2019; Smart and Shea, 2008). Noteworthy that the calculated cut-off rigidity values is a basic reference of charged particle access to different geographical locations and they are very useful for the Space Weather studies and the calculation of the radiation dosesin the atmosphere.

Declaration of Competing Interest

The authors declare that they have no known competing financial interests or personal relationships that could have appeared to influence the work reported in this paper.

Acknowledgments

This work is supported by ESA SSA SWE Space Radiation Expert Service Centre activities (ESA contract number 4000113187/15/D/MRP). It was also partially supported by the Program of the Presidium of RAS No. 3 and No. 28.

Experimentally and methodologically support the project UNU "Russian national network of ground stations of cosmic rays." We are grateful to all staff of the World Network of cosmic ray stations http://cr0.izmiran.ru/ThankYou. The authors from the National and Kapodistrian University of Athens express many thanks to Drs M. A Shea and D.F. Smart for their crucial comments andsuggestions.

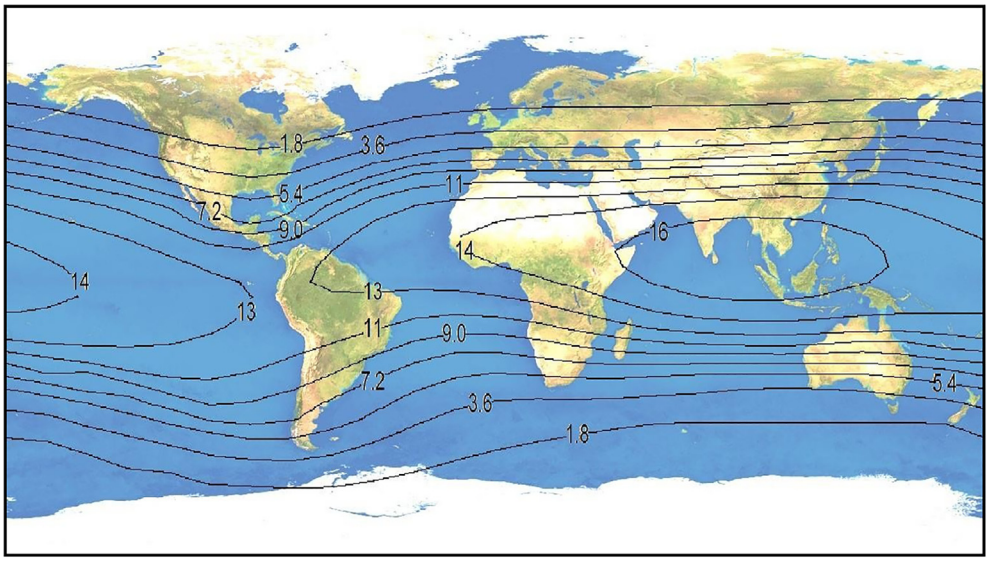

Fig. 4. Map of isodynamic curves of the cut-off rigidity for the year 2020.

References

Alexakis, P., Mavromichalaki, H., 2019. Statistical analysis of interplanetary coronal mass ejections and their geoeffectiveness during the solar cycles 23 and 24. Astrophys. Space Sci. 364, 187. https://doi.org/10.1007/s10509-019-3677-y.

Bütikofer, R., 2018. InSolar particle radiation storms forecasting and analysis. In: Malandraki, O.E., Crosby, N.B. (Eds.), Astrophics and Space Science Library, pp. 79–94..

Gvozdevsky, B., Belov, A., Gushchina, R., Eroshenko, E., Kobelev, P., Yanke, V., 2019. Long-term changes in vertical geomagnetic cutoff rigidities of cosmic rays. Phys. Atomic Nuclei 81, 1382–1389, ISSN 1063-7788.

Dorman, L.I., Gushchina, R.T., Shea, M.A., Smart, D.F., 1972. Cosmic Rays Effective Cut-Off Rigidities, Publishing House "Nauka", Moscow, USSR..

Cooke, D.J., Humble, J.E., Shea, M.A., Smart, D.F., Lund, N., Rasmussen, I.L., Byrnak, B., Goret, P., Petrou, N., 1991. On cosmic-ray cut-off terminology.NuovoCimento C, Serie 1 (ISSN 0390-5551), vol. 14 C, May-June 1991, p. 213-234. Emmanuel College-supported research. DOI: 10.1007/BF02509357..

Friedberg, W., Copeland, K., Duke, F.E., O'Brien, K., Darden, E.B., 1999. Guidelines and technical information provided by the US federal aviation administration to promote radiation safety for air carrier crew members. Radiat. Prot. Dosim. 86, 323–327.

Humble, J.E., Shea, M.A., Smart, D.F., 1985. Sensitivity of cosmic ray trajectory calculations to geomagnetic field model representations. Phys. Earth Planet. Interiors 37 (1), 12–19. https://doi.org/10.1016/0031-9201(85)90058-5.

Kudela, K., Usoskin, I.G., 2004. On magnetospheric transmissivity of cosmic rays. Czech J. Phys. 54, 239–254. https://doi.org/10.1023/B:CJOP.0000014405.61950.e5.

Kudela, K., Bucık, R., Bobık, P., 2008. On transmissivity of low energy cosmic rays in disturbed magnetosphere. Adv. Space Res. 42, 300–1306. https://doi.org/10.1016/j.asr.2007.09.033.

Lewis, B.J., Bennett, L.G.I., Green, A.R., Butler, A., Desormeaux, M., Kitching, F., McCall, M.J., Ellaschuk, B., Pierre, M., 2005. Aircrew dosimetryusing the predictive code for aircrew radiation exposure (PCAIRE). Radiat. Prot. Dosim. 116, 320–326.

Mishev, A., Poluianov, S., Usoskin, I., 2017. Assessment of spectral and angular characteristics of sub-GLE events using the global neutron monitor network. J. Space Weather Space Clim. 7, A28. https://doi.org/10.1051/swsc/2017026.

Model IGRF-12 (2015). ePub. http://www.ngdc.noaa.gov/IAGA/vmod/igrf.html..

Nevalainen, J., Usoskin, I.G., Mishev, A., 2013. Eccentric dipole approximation of the geomagnetic field: Application of the cosmic ray computations. Adv. Space Res. 52, 22–29. https://doi.org/10.1016/j.asr.2013.02.020.

Raukunen, O., Vainio, R., Tylka, A.J., Dietrich, W.F., Jiggens, P., Heynderickx, D., Dierckxsens, M., Crosby, N., Ganse, U., Siipola, R., 2018. Two solar proton fluence models based on ground level enhancement observations. Space Weather Space Clim. 8, A04. https://doi.org/10.1051/swsc/2017031.

Schraube, H., Leuthold, G.P., Heinrich, W., Roesler, S., Combecher, D., 2000. European program package for the calculation of aviation route doses, version 3.0, National Research Center for Environment and Health Institute of Radiation Protection, D-85758, Neuherberg, Germany..

Shea, M.A., Smart, D.F., 1967. Worldwide trajectory-derived vertical cutoff rigidities and their application to experimental measurements for 1955. J. Geophys. Res. 72, 2021–2028. https://doi.org/10.1029/JZ072i007p02021.

Shea, M.A., Smart, D.F., 1975a. Tables of vertical cutoff rigidities for a five degree by fifteen degree a word grid calculated for 1965. AFCRL-TR-75-0381, 524..

Shea M.A., Smart, D. F., 1975b. A five by fifteen degree world grid of calculated cosmic ray vertical cutoff rigidities for 1965 and 1975. In: Proc. 14th ICRC, Munchen, 4, 1298–1303..

Shea, M.A., Smart, D.F., 1983. A world grid of calculated cosmic ray vertical cut-off rigidities for 1980. Proc. 18th ICRC, Bangalore, 3, pp. 514–515.

Shea, M.A., Smart, D.F., 1990. The Influence of the Changing Geomagnetic Field on Cosmic Ray Measurements. J. Geomag. Geoelectr. 42 (1107–1121), 1990.

Shea, M.A., Smart, D.F., 2001. Vertical cut-off rigidities for cosmic ray stations since 1955. In: Proc. 27th ICRC, pp. 4063–4066..

Shea, M.A., Smart, D.F., McCracken, K.G., 1965. A study of vertical cutoff rigidities using sixth degree simulations of the geomagnetic field. J. Geophys. Res. 70, 4117–4130. https://doi.org/10.1029/JZ070i017p041.

Smart, D.F., Shea, M.A., 1997. World grid of calculated cosmic ray vertical cutoff rigidities for epoch 1990.0.Proc. 25th ICRC. Durban. 2, 401–404.

Smart, D.F., Shea, M.A, 2000. Geomagnetic Cutoff Rigidity Computer Program, Final Report, Grant NAG5-8009, Center for Space Plasmas and Aeronomic Research, University of Alabama in Huntsville..

Smart, D.F., Shea, M.A., 2006. Vertical Geomagnetic Cutoff Rigidities for Epoch 2000—Deviations from Expected Latitude Curves Advances in Geosciences. Volume 2: Solar Terrestrial (ST). Published by World Scientific. ISBN #978-981-2707-18-5, 2006, pp. 277–285..

Smart, D.F., Shea, M.A., 2007. World grid of calculated cosmic ray vertical cutoff rigidities for Epoch 1995. Proc. 30th ICRC, Mexico, 1, pp. 733–736.

Smart, D.F., Shea, M.A., 2008. World grid of calculated cosmic ray vertical cutoff rigidities for Epoch 2000.0. Proc. 30th ICRC, Mexico, 1, pp. 737–740.

Smart, D.F., Shea, M.A., 2009. Fifty Years of progress in geomagnetic cut-off rigiditydeterminations. Adv. Space Res. 44, 1107–1123.

Smart, D.F., Shea, M.A., 2019. Vertical geomagnetic cut off rigidities for Epoch 2015. In: PoS 36th ICRC Madison, WI, USA, 36. 1154S.

Smart, D.F., Shea, M.A., Flückiger, E.O., 2000. Magnetospheric models and trajectory computations. Space Science Rev. 93, 305–333. https://doi.org/10.1023/A:1026556831199.

Tezari, A., Paschalis, P., Mavromichalaki, H., Karaiskos, P., Crosby, N., Dierckxsens, M., 2020. Assessing radiation exposure inside the Earth's atmosphere. Radiation Protection Dosimetry. https://doi.org/10.1093/rpd/ncaa112.

Stormer, C., 1930. Periodische Elektronenbahnenim Feldeeines Elementarmagneten und ihre Anwendung auf Brüches Modellversuche und auf Eschenhagens Elementarwellen des Erdmagnetismus. Mit 32 Abbildungen, Zeitschriftfür Astrophysik 1, 237..

Thébault, E., Finlay, C., Zvereva, T., 2015. International Geomagnetic Reference Field: the 12th generation. Earth Planets Space 67, 79.

Tsyganenko, N., 1989. A magnetospheric magnetic field model with a warped tail current sheet. Planet. Space Sci. 37 (1), 50–120.

Zi-Gang, Wei, Xu, Wen-yao, 2001. Drifts and Intensity Variations of the Geomagnetic Field. Chin. J. Geophys. 44, 496. https://doi.org/10.1002/cjg2.167.

Zreda, M., 2012. COSMOS project University of Arizona. Cutoff rigidity online Calculator, model IGRF. Epub.